ORIGINAL ARTICLE

Open Access

Face Grinding Surface Quality of High Volume Fraction SiC$_p$/Al Composite Materials

Xu Zhao[1,2] , Yadong Gong[1*], Guiqiang Liang[3], Ming Cai[1] and Bing Han[2]

Abstract

The existing research on SiC$_p$/Al composite machining mainly focuses on the machining parameters or surface morphology. However, the surface quality of SiC$_p$/Al composites with a high volume fraction has not been extensively studied. In this study, 32 SiC$_p$/Al specimens with a high volume fraction were prepared and their machining parameters measured. The surface quality of the specimens was then tested and the effect of the grinding parameters on the surface quality was analyzed. The grinding quality of the composite specimens was comprehensively analyzed taking the grinding force, friction coefficient, and roughness parameters as the evaluation standards. The best grinding parameters were obtained by analyzing the surface morphology. The results show that, a higher spindle speed should be chosen to obtain a better surface quality. The final surface quality is related to the friction coefficient, surface roughness, and fragmentation degree as well as the quantity and distribution of the defects. Lower feeding amount, lower grinding depth and appropriately higher spindle speed should be chosen to obtain better surface quality. Lower feeding amount, higher grinding depth and spindle speed should be chosen to balance grind efficiently and surface quality. This study proposes a systematic evaluation method, which can be used to guide the machining of SiC$_p$/Al composites with a high volume fraction.

Keywords: SiC$_p$/al, Face grinding, Grinding force, Friction coefficient, Surface morphology

1 Introduction

SiC$_p$/Al is a composite material with high specific stiffness, specific strength, and thermal conductivity, and a low thermal expansion coefficient. Therefore, it is widely used in precision optical instruments, advanced weapons, and the aerospace field [1–4]. In the aerospace field, SiC$_p$/Al is widely used in optical structure components and electronic packaging systems. To satisfy the application requirements, SiC$_p$/Al composites with a high volume fraction are needed [5, 6]; they have excellent mechanical properties. However, SiC particles exhibit high levels of hardness and strength. Consequently, SiC$_p$/Al composites with a high volume fraction are difficult to machine [7–9]. To expand the application of SiC$_p$/Al composites with a high volume fraction, many studies have been

conducted by researchers worldwide. Additionally, many research results have been obtained [10–13].

Ciftci et al. [14] conducted a research on the effect of the volume fraction and particle size on cutting tool wear. The results showed that coated carbide tools had a longer service life. To predict the cutting force during the orthogonal cutting of SiC$_p$/Al composite materials, Kishawy et al. [15] proposed a force model based on energy analysis. Some scholars conducted a research on the effect of the machining parameters and cutting tool structure on the cutting process [16–18]. Zheng et al. [19] studied the surface roughness of SiC$_p$/Al composite materials after vibration grinding. The results showed that the spindle speed was the most influential machining parameter. The surface fractal dimension was related to the spindle speed and feeding velocity. Additionally, the surface defects had a significant influence on the surface fractal dimension. Du et al. [20] studied the chip formation mechanism during the grinding of SiC$_p$/Al composite materials,

*Correspondence: gongyd@mail.neu.edu.cn
[1] School of Mechanical Engineering and Automation, Northeastern University, Shenyang 110819, China
Full list of author information is available at the end of the article

Zhao *et al. Chin. J. Mech. Eng.*   (2021) 34:3

Page 2 of 14

and the topography characteristics of the chips were observed by a scanning electron microscope (SEM). The results showed that flake chips were the most common type. Kannan et al. [21] studied the formation mechanism of serrated chips during the machining of SiC_p/Al composite materials. The results showed that stress was concentrated in the contact area between the aluminum matrix and SiC particles. Therefore, key holes were formed in the contact area and serrated chips were generated. Besides, a few researchers carried out single grit scratch tests to investigate SiCp/Al composites removal characteristics [22, 23].

According to the references, SiC_p/Al composite materials can be precisely machined [24–30]. However, the machining parameters were not comprehensively analyzed, and the surface morphology was not systematically evaluated in these references. Taking the spindle speed, feeding amount, and grinding depth as the machining parameters, 32 SiC_p/Al specimens were grinding machined. The specimens were grouped and their surface quality was analyzed by the cutting force, friction coefficient, and roughness parameters. Further, the grinding qualities of the specimens were analyzed.

## 2 Testing Process and Detection

2.1 Testing Process

As shown in Figure 1(a), the testing system was based on an ultrasonic machine tool. The electroplated diamond wheel in Figure 1(b) was used as the grinding tool. The outer diameter and wall thickness of the grinding tool were 12 mm and 2 mm, respectively. The particle size of the diamond grain was D126 (120/140). The matrix and particle-reinforced materials of the workpieces were Al 2024-T6 and SiC ceramic, respectively. The particle volume fraction and average size of SiC were 62.5% and 40 μm, respectively. The rest of the parameters are listed in Table 1.

The specimens are shown in Figure 1(c). The upper surface was selected as the testing surface and the dimensions of the specimens were 3 mm×8 mm×10 mm. The cooling fluid supplied by Blaser was used for the testing system; the processing parameters are listed in Table 2. All the tests were conducted twice and the average experimental values were obtained.
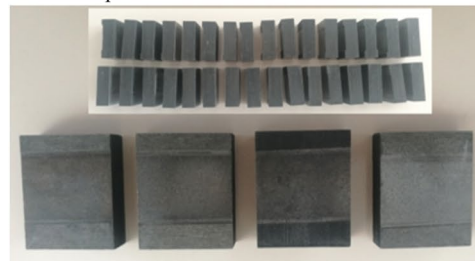
2.2 Detection Method

As shown in Figure 1(b), the Kistler 9257B was used to measure the grinding forces, and the data sampling frequency was set at 9 kHz. All the machined surfaces were washed by the ultrasonic cleaning method before
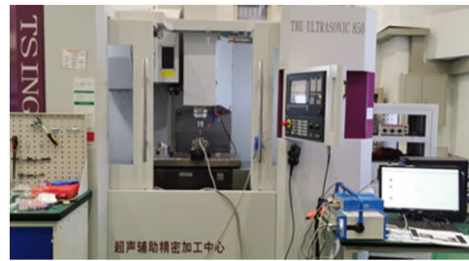
a Testing system
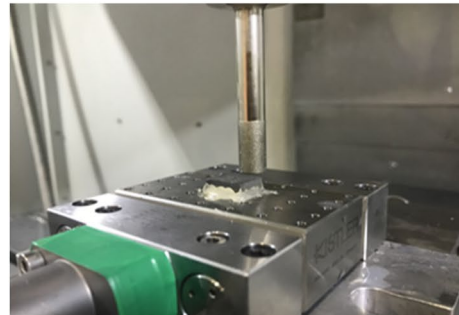
b Electroplated diamond wheel and Kistler 9257B

c Experimental specimens

d VK-X 3D laser scanning microscope

Figure 1 Experimental equipment

Zhao *et al. Chin. J. Mech. Eng.* (2021) 34:3

Page 3 of 14

Table 1 Parameters of SiC and Al 2024-T6

Material	SiC	Al 2024-T6
Elastic modulus (GPa)	420	74.2
Poisson ratio	0.14	0.33
Yield stress (MPa)	5700	345.4
Density (kg/m^3)	3130	2780
Heat capacity (J/kg·°C)	427	875

Table 2 Processing parameters

No.	Spindle speed (r/min)	Feeding amount (mm/min)	Grinding depth (μm)
T1	2000	50	5
T2	2000	50	20
T3	2000	50	40
T4	2000	50	80
T5	4000	50	5
T6	4000	50	20
T7	4000	50	40
T8	4000	50	80
T9	6000	50	5
T10	6000	50	20
T11	6000	50	40
T12	6000	50	80
T13	8000	50	5
T14	8000	50	20
T15	8000	50	40
T16	8000	50	80
T17	2000	100	5
T18	2000	100	20
T19	2000	100	40
T20	2000	100	80
T21	4000	100	5
T22	4000	100	20
T23	4000	100	40
T24	4000	100	80
T25	6000	100	5
T26	6000	100	20
T27	6000	100	40
T28	6000	100	80
T29	8000	100	5
T30	8000	100	20
T31	8000	100	40
T32	8000	100	80

the surface topography measurement. As shown in Figure 1(d), a VK-X 3D laser scanning microscope was used to determine the distribution of the surface defects. Additionally, the parameters of the surface topography can be analyzed systematically.

3 Evaluation Standard

To evaluate the machining quality, the grinding force (F), friction coefficient (COF), roughness parameters, and surface morphology were chosen as the evaluation parameters. The specimens were machined by the face-grinding method, and the axial grinding force was obtained as an evaluation parameter. The friction coefficient was used to evaluate the friction condition between the machine tool and specimen. The higher the value of the friction coefficient, the worse the surface quality.

The following parameters were chosen as the roughness parameters: surface roughness (Ra), broken area ratio (S_{dr}), peak height (R_p), lowest valley (R_v), gradient (S_{sk}) and kurtosis (S_{ku}). The parameters are defined as follows.

(1) Ra is the arithmetic average roughness, which represents the arithmetical mean deviation of the profile.

(2) S_{dr} is used to evaluate the fragmentation degrees of the surfaces after grinding. The higher the value of S_{dr}, the larger the fragmentation area.

(3) R_p and R_v are the peak height and lowest valley of the profile, respectively.

(4) S_{sk} is used to evaluate the profile amplitude distribution. It is equal to 0 if the height of the profile surface is symmetrically distributed, less than 0 if low valleys exist below the middle plane, and higher than 0 if peaks exist above the middle plane.

(5) S_{ku} is the kurtosis of the surface height distribution. S_{ku} is less than 3 if the surface profile is flat and more than 3 if the surface profile is steep.

4 Results and Discussion

4.1 Experimental Results

As presented in Table 3, the experiments were divided into eight groups according to the feeding amount, grinding depth, and spindle speed. The experimental results of the grinding force (F), friction coefficient (COF), and roughness parameters are listed in Table 3.
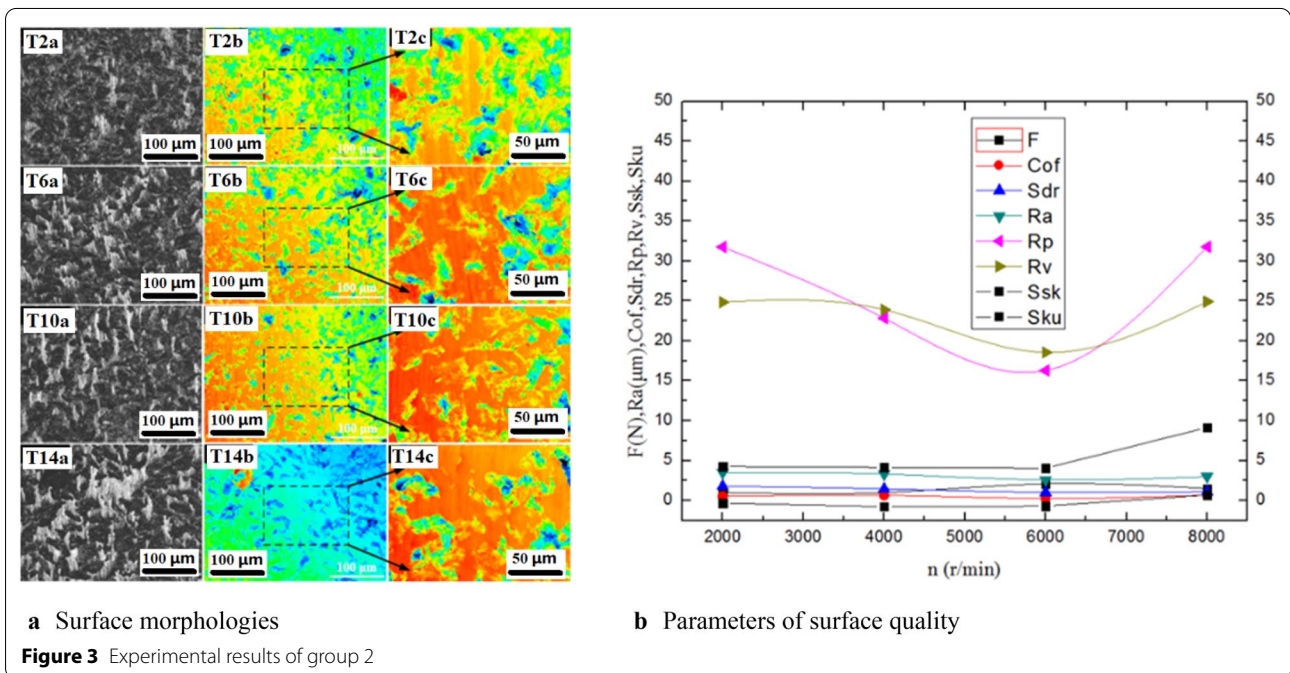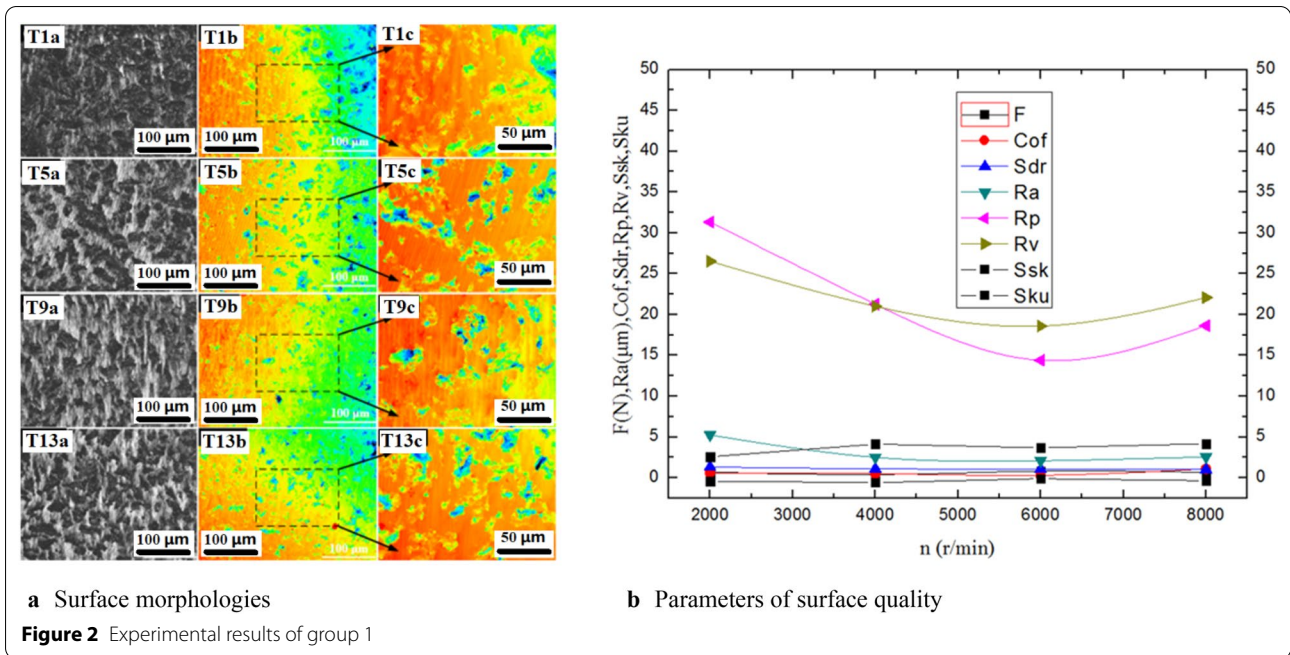
Zhao *et al. Chin. J. Mech. Eng.*   (2021) 34:3

Page 4 of 14

Table 3 Parameters of surface quality

No.	Group	Feeding amount (mm/min)	Grinding depth (μm)	Spindle speed (r/min)	F	COF	S_{dr}	Ra	R_p	R_v	S_{sk}	S_{ku}
T1	1	50	5	2000	0.70	0.57	1.33	5.26	31.34	26.54	−0.41	2.57
T5				4000	0.40	0.5	1.09	2.51	21.27	21.03	−0.58	4.13
T9				6000	0.80	0.29	1.06	2.08	14.39	18.59	−0.11	3.68
T13				8000	0.65	0.71	1.02	2.56	18.64	22.08	−0.35	4.17
T2	2		20	2000	1.00	0.51	1.80	3.50	31.76	24.85	−0.34	4.27
T6				4000	1.00	0.65	1.46	3.30	22.83	23.90	−0.75	4.16
T10				6000	2.10	0.30	1.02	2.59	16.29	18.55	−0.69	4.05
T14				8000	1.50	0.67	1.10	2.99	31.78	24.92	0.70	9.15
T3	3		40	2000	2.00	0.42	1.79	3.53	27.51	27.13	−0.33	3.90
T7				4000	2.85	0.32	1.24	2.94	26.74	32.04	−0.75	4.75
T11				6000	3.00	0.37	1.00	3.49	17.12	33.53	−2.53	12.01
T15				8000	2.10	0.57	1.08	2.40	20.42	21.16	−0.68	4.68
T4	4		80	2000	3.50	0.46	1.30	4.72	52.12	48.39	−0.49	3.98
T8				4000	3.80	0.49	1.39	2.62	32.61	22.54	−0.34	4.13
T12				6000	8.00	0.44	0.93	2.05	13.97	21.85	−0.78	4.70
T16				8000	5.60	0.29	0.98	2.13	13.83	21.16	−0.37	4.29
T17	5	100	5	2000	1.20	0.25	1.11	2.51	17.61	22.70	−0.37	3.69
T21				4000	1.50	0.20	0.89	2.03	14.54	25.51	−0.57	4.93
T25				6000	1.55	0.17	1.13	2.39	13.80	14.30	−0.16	2.70
T29				8000	0.55	0.27	1.12	2.14	14.47	17.14	−0.30	2.89
T18	6		20	2000	2.10	0.24	1.38	3.15	29.05	25.96	−0.76	4.65
T22				4000	1.80	0.19	1.13	2.80	19.98	22.01	−0.77	4.37
T26				6000	2.75	0.22	1.09	2.44	22.77	17.01	−0.40	3.39
T30				8000	3.00	0.24	1.06	3.43	18.6	25.47	−0.65	4.91
T19	7		40	2000	3.75	0.19	1.32	3.04	22.09	23.75	−0.68	4.37
T23				4000	5.15	0.30	1.07	2.73	19.28	22.32	−0.86	4.37
T27				6000	3.50	0.36	1.19	3.03	19.62	22.70	−0.30	2.91
T31				8000	4.25	0.31	1.32	2.56	15.31	20.72	−0.16	2.91
T20	8		80	2000	7.50	0.37	1.19	2.57	18.45	25.34	−1.23	6.00
T24				4000	8.00	0.38	1.20	2.34	21.08	22.37	−0.87	5.47
T28				6000	6.50	0.38	1.24	3.61	19.69	20.60	−0.03	2.26
T32				8000	5.25	0.35	1.18	2.29	18.06	19.52	−0.55	4.03

4.2 Surface Quality under Lower Feeding Amount and Cutting Depth

The surface morphologies of groups 1 and 2 are shown in Figure 2(a) and Figure 3(a), respectively. The four photos on the left are the scanning electron microscope (SEM) results, whereas those in the middle show the height distribution of the surface morphology. We can obtain the four photos on the right by enlarging the central areas of the four photos in the middle. The lower areas are shown in black and blue, and the higher areas are in red. The surface quality parameters of groups 1 and 2 are shown in Figure 2(b) and Figure 3(b), respectively.

From Figure 2 and Figure 3, it can be observed that the experimental results of T9 and T10 are relatively superior to those of the other specimens. Core areas of the specimens were selected to compare the grinding qualities of T9 and T10; a magnified three-dimensional profile of the core areas is shown in Figure 4. The average roughness (Ra) and best roughness (Rab) of the core areas were determined. All the experimental parameters are listed in Table 4.
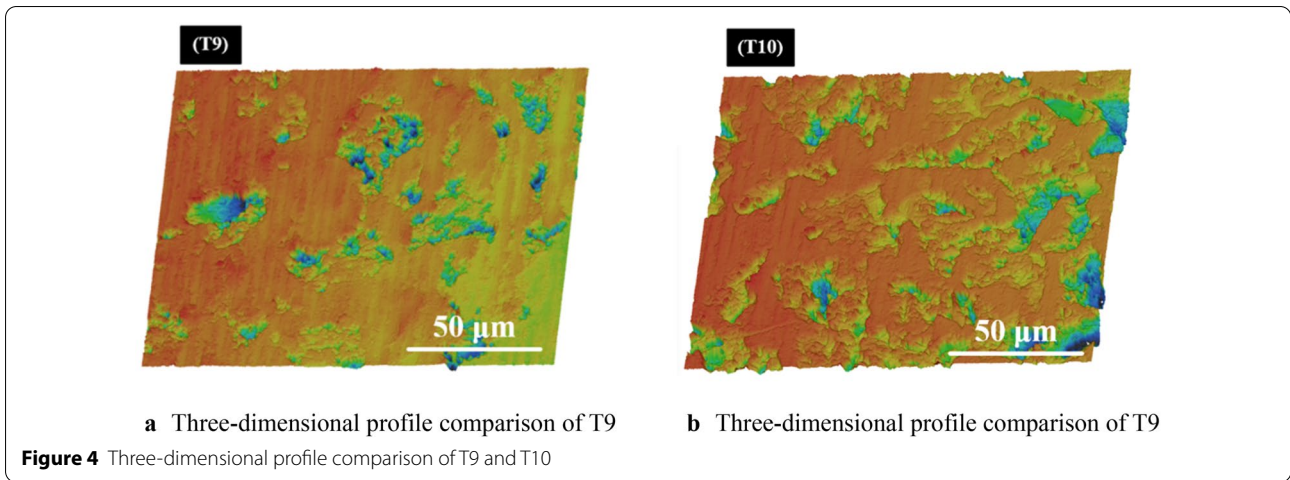
Zhao *et al. Chin. J. Mech. Eng.*   (2021) 34:3

Page 5 of 14

a Surface morphologies

b Parameters of surface quality

Figure 2 Experimental results of group 1

a Surface morphologies

b Parameters of surface quality

Figure 3 Experimental results of group 2

Zhao *et al. Chin. J. Mech. Eng.* (2021) 34:3

Page 6 of 14

a Three-dimensional profile comparison of T9

b Three-dimensional profile comparison of T9

Figure 4 Three-dimensional profile comparison of T9 and T10

Table 4 Experimental parameters comparison of T9 and T10

No.	T9	T10
Feeding amount (mm/min)	50	50
Grinding depth (µm)	5	20
Spindle speed (r/min)	6000	6000
F	0.80	2.10
COF	0.29	0.30
S_{dr}	1.06	1.02
Ra	2.08	2.59
Rab	0.26	0.31
R_p	14.39	16.29
R_v	18.59	18.55
S_{sk}	−0.11	−0.69
S_{ku}	3.68	4.05

From Figure 4, it can be observed that the surface morphology of T9 is relatively flat. Table 4 shows that the experimental parameters of T9 are relatively superior to those of T10. Therefore, the surface quality of T9 is the best in groups 1 and 2. This mechanism can be explained as follows. The feeding amount, grinding depth, and spindle speed of T9 are 50 mm/min, 5 µm and 6000 r/min, respectively. The average diameter of SiC particles is 40 µm. The particles are relatively steady when the grinding depth is 5 µm. However, the particles are pulled out with the increase of grinding depth, causing the appearance of pits on the grinding surface.

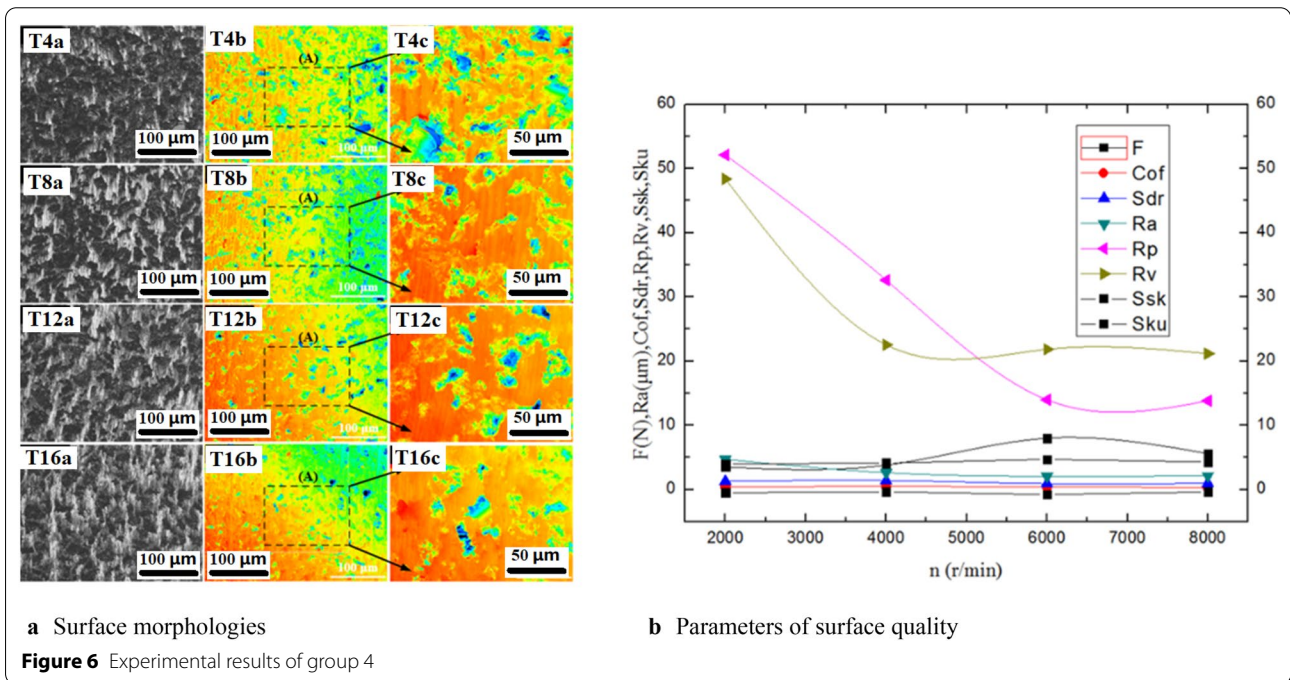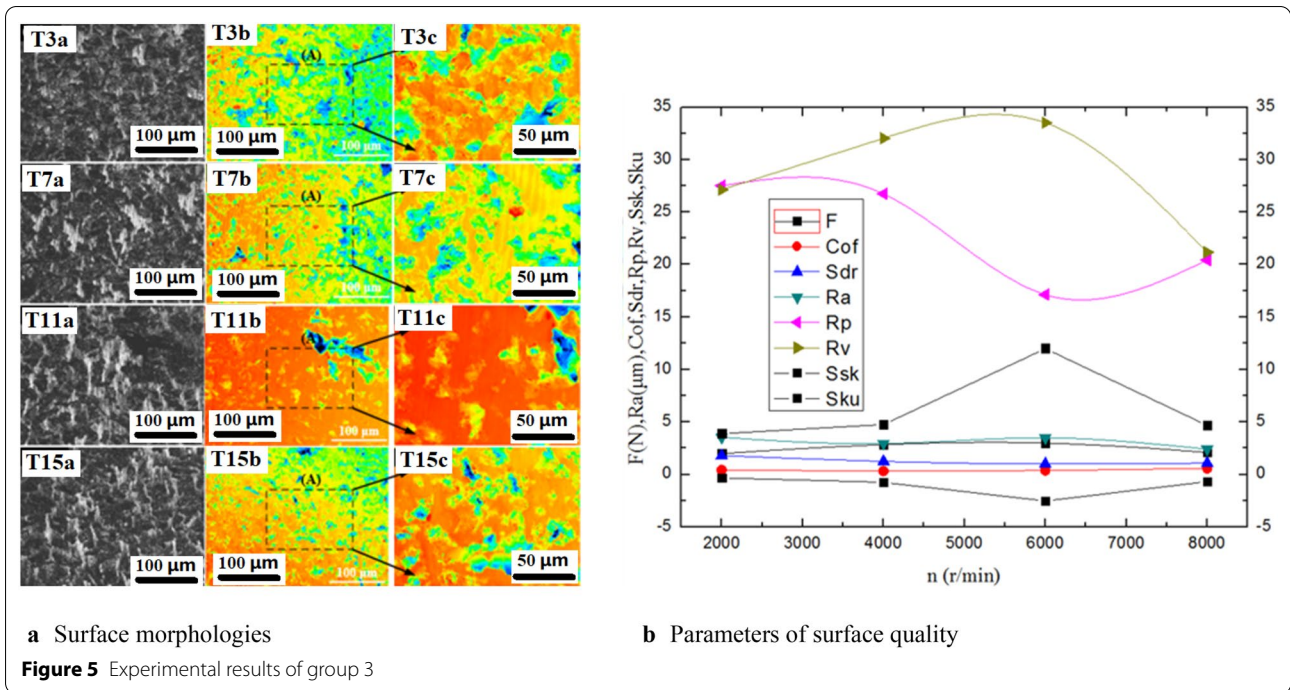### 4.3 Surface Quality under Lower Feeding Amount and Larger Cutting Depth

The surface morphologies of groups 3 and 4 are shown in Figure 5(a) and Figure 6(a), respectively. Moreover, the surface quality parameters of groups 3 and 4 are shown in Figure 5(b) and Figure 6(b), respectively.

From Figure 5, it can be observed that many pits exist on the surfaces of T3 and T7, indicating that their flatness is very poor. The S_{sk} and S_{ku} of T11 are −2.53 and 12.01, respectively. This indicates that the surface of T11 was depressed, and had deep pits. Therefore, the surface quality of T15 is the best in group 3.

From Figure 6, the S_{dr} and R_v of T4 and T8 are relatively high. This indicates that many surface defects and deep pits exist on the surface. Moreover, the S_{sk} and S_{ku} of T12 are relatively high, which indicates that the surface defects exist and the profile of T12 is very sharp. Therefore, the surface quality of T16 is the best in group 4.

Core areas of the specimens were selected to compare the grinding quality of T15 and T16. The magnified three-dimensional profiles of the core areas are shown in Figure 7. The Ra and Rab of the core areas were determined. All the experimental parameters are listed in Table 5.

As can be observed from Figure 7, the surface morphology of T16 is relatively flat. Table 5 shows that the experimental parameters of T16 are relatively superior to those of T15. Therefore, the surface quality of T16 is the best in groups 3 and 4. The mechanism can be
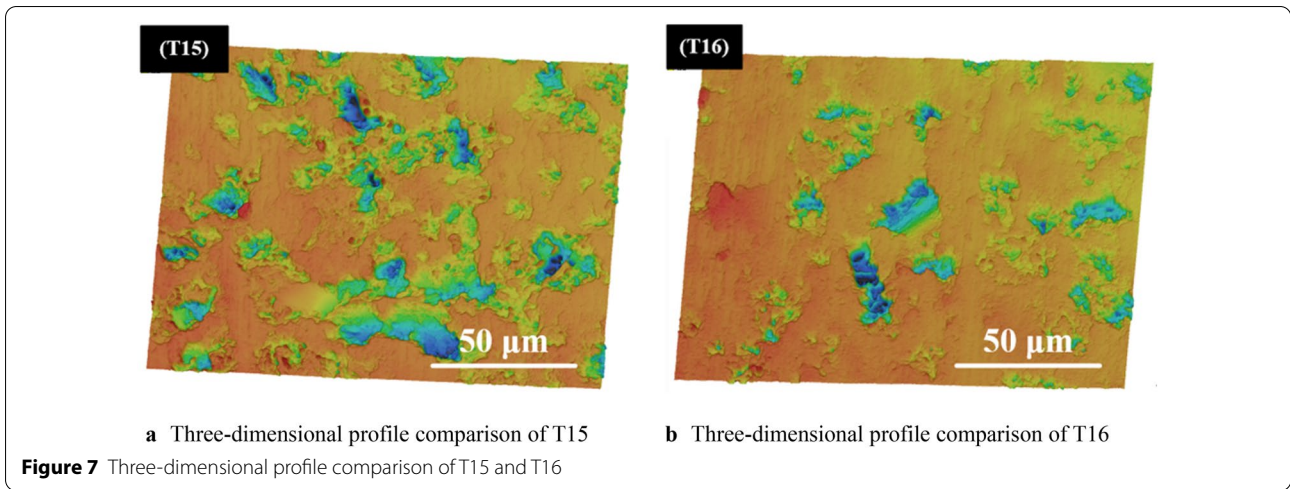
Zhao *et al. Chin. J. Mech. Eng.* (2021) 34:3

Page 7 of 14

a Surface morphologies

b Parameters of surface quality

Figure 5 Experimental results of group 3

a Surface morphologies

b Parameters of surface quality

Figure 6 Experimental results of group 4

Zhao *et al. Chin. J. Mech. Eng.* (2021) 34:3

Page 8 of 14

a Three-dimensional profile comparison of T15 **b** Three-dimensional profile comparison of T16

Figure 7 Three-dimensional profile comparison of T15 and T16

Table 5 Experimental parameters comparison of T15 and T16

Parameter	T15	T16
Feeding amount (mm/min)	50	50
Grinding depth (μm)	40	80
Spindle speed (r/min)	8000	8000
F	2.10	5.60
COF	0.57	0.29
S_{dr}	1.08	0.98
Ra	2.4	2.13
Rab	0.29	0.26
R_p	20.42	13.83
R_v	21.46	21.16
S_{sk}	−0.68	−0.37
S_{ku}	4.68	4.29

explained as follows. The feeding amount, grinding depth, and spindle speed of T16 are 50 mm/min, 80 μm and 8000 r/min, respectively. The average diameter of the SiC particles is 40 μm, and 80 μm is twice the size of the average diameter. Theoretically speaking, SiC particles can be pulled out entirely. However, the particles are irregular and differences exist between the protrusion heights of the diamond particles. Therefore, different surface morphologies appear with the change in grinding parameters.

4.4 Surface Quality under Larger Feeding Amount and Lower Cutting Depth
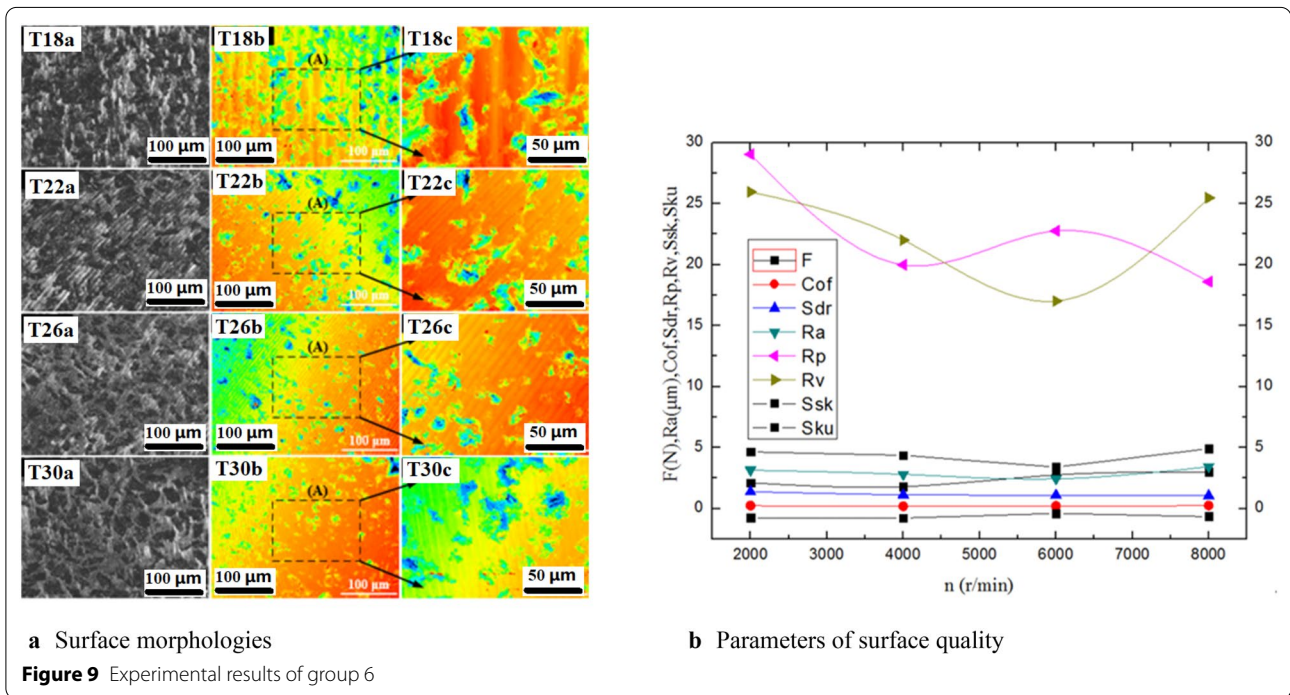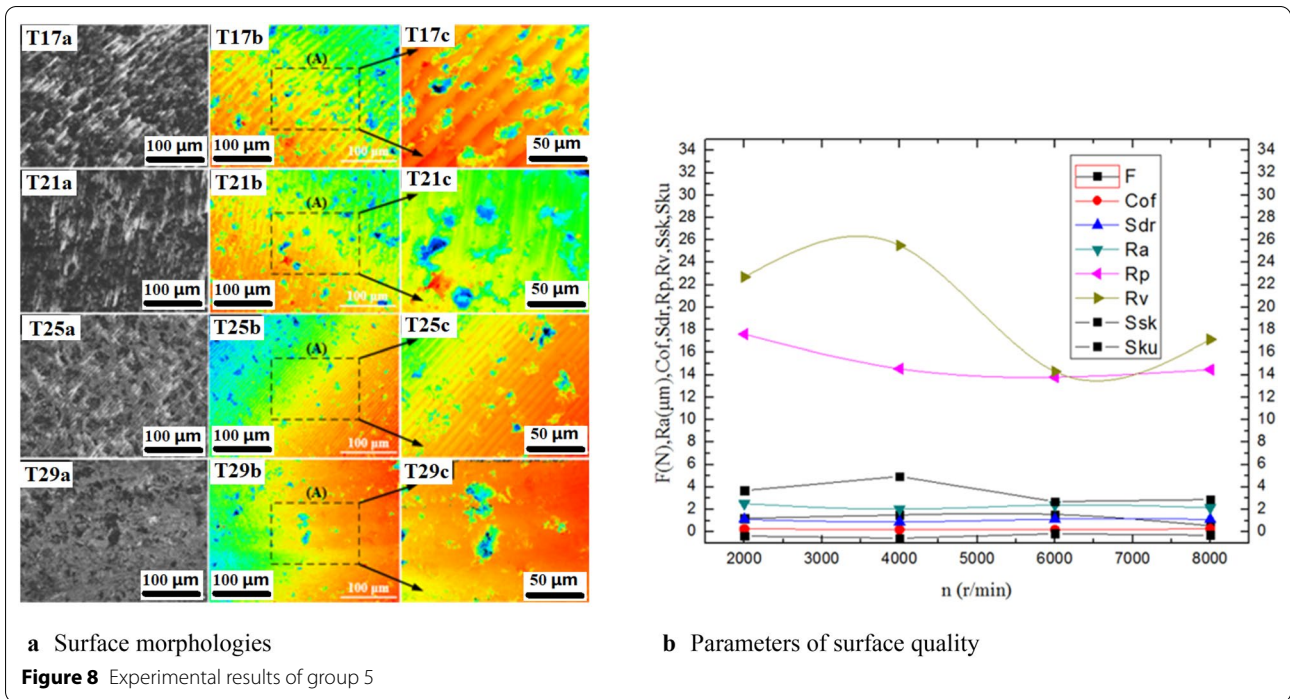
The surface morphologies of groups 5 and 6 are shown in Figure 8(a) and Figure 9(a), respectively. Moreover, their surface quality parameters are shown in Figure 8(b) and Figure 9(b), respectively.

As can be observed from Figure 8, the surface morphology of T25 is relatively superior to that of T17, T21, and T29. Figure 9 shows that the surface morphology of T26 is relatively superior to that of T18, T22, and T30. Core areas of the specimens were selected to compare the grinding qualities of T25 and T26. The magnified three-dimensional profiles of the core areas are shown in Figure 10. The Ra and Rab of the core areas were determined. All the experimental parameters are listed in Table 6.

As can be observed from Figure 10, the surface morphology of T25 is relatively flat. Table 6 shows that the experimental parameters of T25 are relatively superior to those of T26. Therefore, the surface quality of T25 is the best in groups 5 and 6. The feeding amount, grinding depth, and spindle speed of T25 are 100 mm/min, 5 μm and 6000 r/min, respectively.

4.5 Surface Quality under Larger Feeding Amount and Larger Cutting Depth

The surface morphologies of groups 7 and 8 are shown in Figure 11(a) and Figure 12(a), respectively.
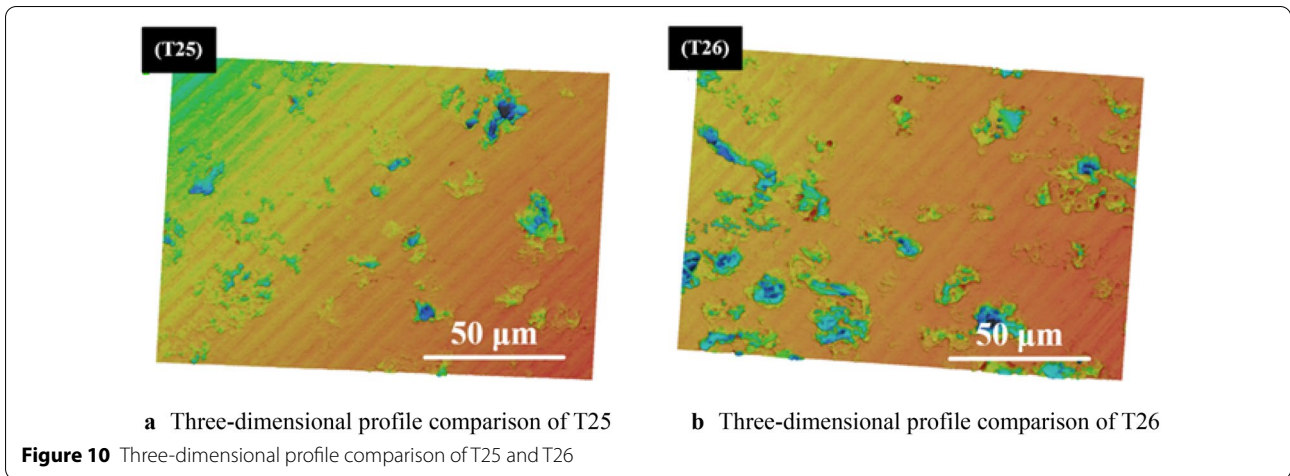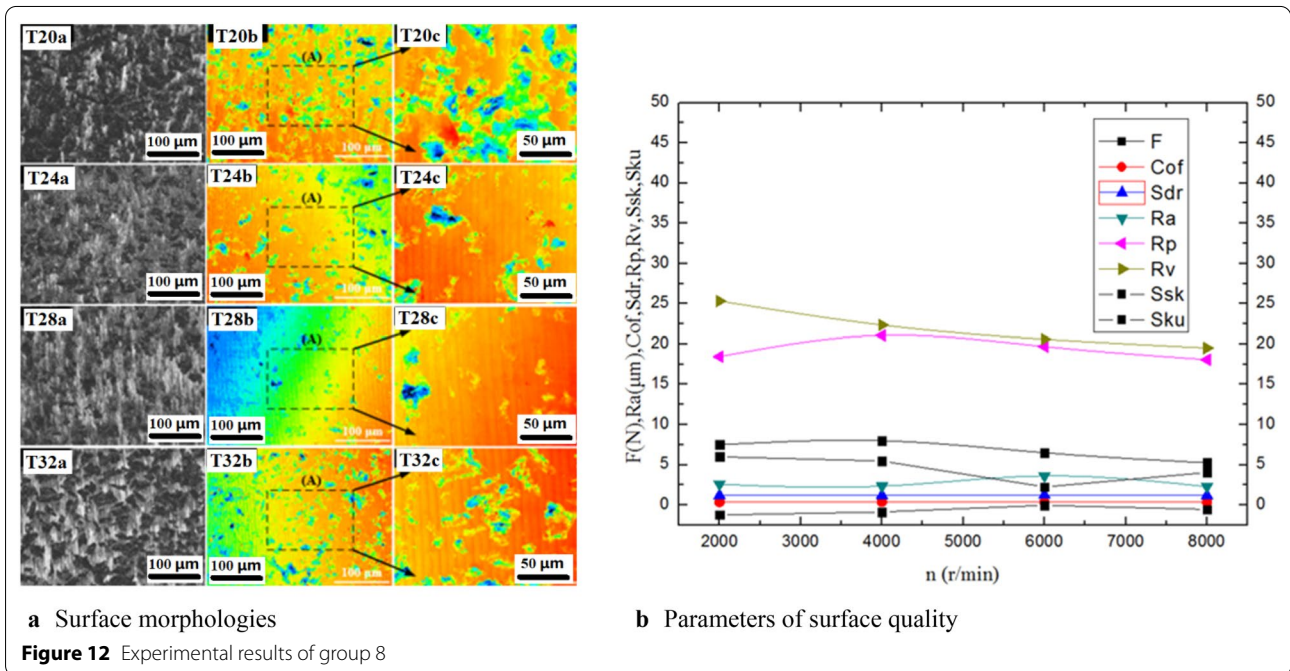
a Surface morphologies **b** Parameters of surface quality

Figure 8 Experimental results of group 5

a Surface morphologies **b** Parameters of surface quality

Figure 9 Experimental results of group 6

Zhao *et al. Chin. J. Mech. Eng.* (2021) 34:3

Page 10 of 14

a Three-dimensional profile comparison of T25

b Three-dimensional profile comparison of T26

Figure 10 Three-dimensional profile comparison of T25 and T26

Table 6 Experimental parameters comparison of T25 and T26

Parameter	T25	T26
Feeding amount (mm/min)	100	100
Grinding depth (µm)	5	20
Spindle speed (r/min)	6000	6000
F	1.55	2.75
COF	0.17	0.22
S_{dr}	1.13	1.09
Ra	2.39	2.44
Rab	0.31	0.32
R_p	13.80	22.77
R_v	14.3	17.01
S_{sk}	−0.16	−0.4
S_{ku}	2.70	3.39

Moreover, their surface quality parameters are shown in Figure 11(b) and Figure 12(b), respectively.

From Figure 11 and Figure 12, it can be observed that the surface qualities of T27 and T28 are relatively superior to those of other specimens by comprehensive considerations of the experimental parameters and surface morphologies.

Core areas of the specimens were selected to compare the grinding qualities of T27 and T28. The magnified three-dimensional profiles of the core areas are shown in Figure 13. The Ra and Rab of the core areas were determined. All the experimental parameters are listed in Table 7.

As can be observed from Figure 13, many pits exist on the surface of T27. However, the pits are not very deep. This may be because of the pulling out of SiC. Table 7 shows that the S_{dr}, Ra, Rab and Rp of T27 is lower than that of T28. On the whole, surface parameters of T27 are

a Surface morphologies

Figure 11 Experimental results of group 7

b Parameters of surface quality

a Surface morphologies

Figure 12 Experimental results of group 8

b Parameters of surface quality
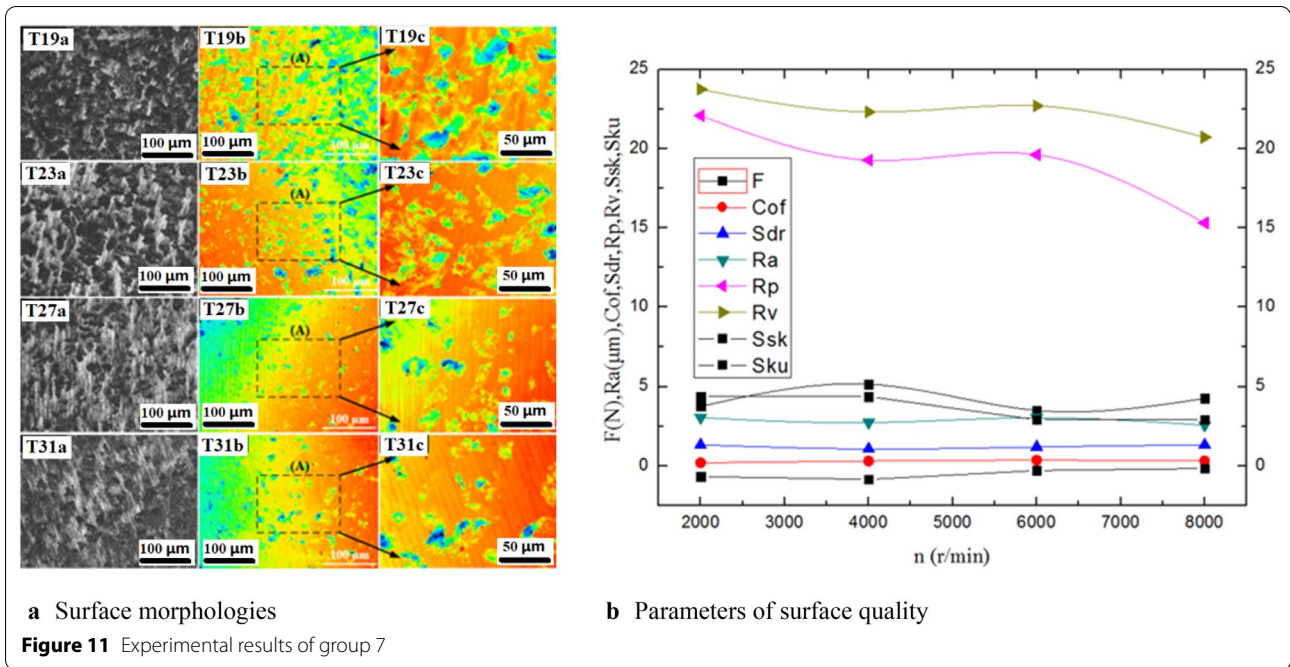
relatively superior to those of T28. Therefore, the surface quality of T27 is the best in groups 7 and 8.

4.6 Three-dimensional Profile Comparison

According to the above analysis, T9, T16, T25, and T27 are relatively superior to the other specimens. The three-dimensional profiles of these four specimens are shown in Figure 14.

a Three-dimensional profile comparison of T27   **b** Three-dimensional profile comparison of T28

Figure 13 Three-dimensional profile comparison of T27 and T28
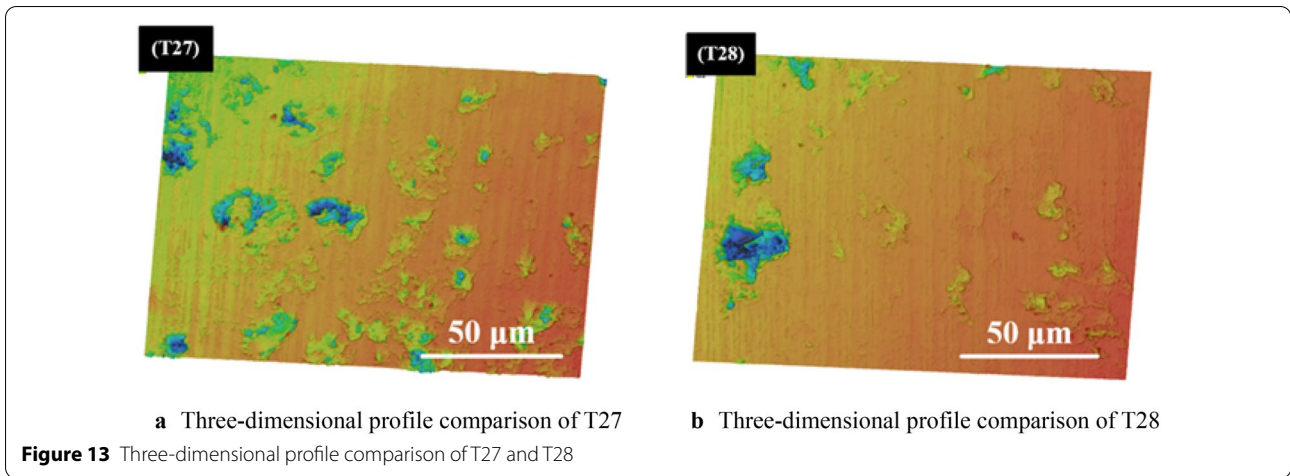
Table 7 Experimental parameters comparison of T27 and T28

Parameter	T27	T28
Feeding amount (mm/min)	50	50
Grinding depth (μm)	40	80
Spindle speed (r/min)	6000	6000
F	3.50	6.5
COF	0.36	0.38
S_{dr}	1.19	1.24
Ra	3.03	3.61
Rab	0.19	0.22
R_p	19.62	19.69
R_v	22.70	20.60
S_{sk}	−0.30	−0.03
S_{ku}	2.91	2.26

As shown in Figure 14, surface quality of T9 is best, lower feeding amount, lower cutting depth and appropriately higher spindle speed should be recommended to obtain better surface quality. As shown in Figure 14(c) and (d), obvious feeding marks appears on surfaces of T25 and T27, which should be avoided, so lower feeding amount, higher cutting depth and higher spindle speed should be recommended to balance grinding efficiency and surface quality.

5 Conclusions

(1) In this study, 32 SiCp/Al specimens with a high volume fraction were prepared and their machining parameters were measured. The surface quality of the specimens was tested, and the effect of the grinding parameters on the surface quality of the SiCp/Al composites was analyzed.

(2) Taking the grinding force, friction coefficient, and roughness parameters as the evaluation standards,

the surface quality of the specimens under different machining parameters was analyzed. To obtain better surface quality, lower feeding amount, lower cutting depth and appropriately higher spindle speed should be chosen. To balance grinding efficiency and surface quality, lower feeding amount, higher cutting depth and spindle speed should be chosen.

(3) This study comprehensively analyzed machining parameters and systematically evaluated the surface morphology of SiCp/Al specimens with a high volume fraction. However, more research work should be conducted in the future. For example, the surface morphology from the view of material properties, and the influence of machining parameters should be fully discussed in the future.
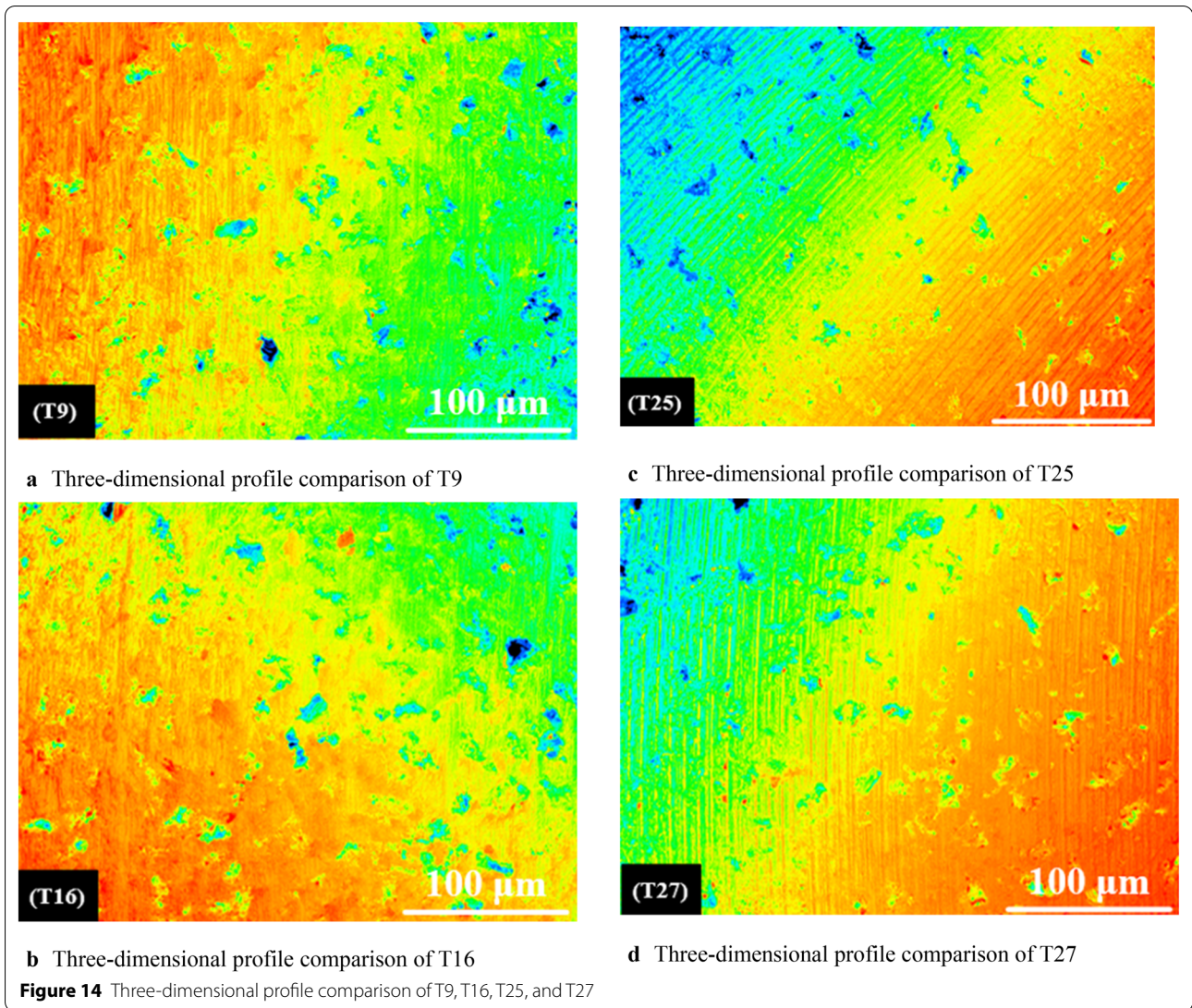
Authors' Information
Xu Zhao, born in 1982, is currently a PhD candidate at *School of Mechanical Engineering and Automation*, *Northeastern University*, *China*, as well as an associate professor at *School of Mechanical Engineering and Automation*, *University of Science and Technology Liaoning*, *China*. His main research interests include grinding and precision machining, modern mechanical design theory and method, and bionic engineering. E-mail: 1982zhaoxu@163.com, zx@ustl.edu.cn.

Yadong Gong, born in 1958, is a professor at *School of Mechanical Engineering and Automation*, *Northeastern University*, *China*. He has served as dean of the department and dean of the school of mechanical engineering and automation. He holds a master's degree in engineering and a doctorate in engineering from *Northeastern University*. Currently he is a member of ICAT and Vice Chairman of *Liaoning Institute of Mechanical Engineering*. Since 1995, he has been engaged in mechanical manufacturing and automation research.

Zhao *et al. Chin. J. Mech. Eng.*   (2021) 34:3

Page 13 of 14

a Three-dimensional profile comparison of T9

c Three-dimensional profile comparison of T25

b Three-dimensional profile comparison of T16

d Three-dimensional profile comparison of T27

Figure 14 Three-dimensional profile comparison of T9, T16, T25, and T27

Especially in grinding and precision machining, digital manufacturing and micro-scale machining and other aspects of a number of research results. In recent years, he has carried out research work and made progress in the grinding of special difficult materials and robot grinding. E-mail: gongyd@mail.neu.edu.cn.

Guiqiang Liang, born in 1976, head of the team of *Linghang Kegong*, is a professional leader in the field of cutting simulation and a promoter of industry-university-research cooperation. Liang is postgraduate tutor of *Tsinghua University*, senior engineer of *Chinese Academy of Sciences*, senior member of *China Mechanical Engineering Society*, science and technology project evaluation expert of *Science and Technology Department in Zhejiang and Hunan*, and also think tank expert for high-end equipment manufacturing and military-civilian integration of *Xiangtan City, Hunan Province*. E-mail: 13910401904@163.com.

Ming Cai, born in 1990, is currently a PhD candidate at *School of Mechanical Engineering and Automation*, *Northeastern University*, *China*. His main research interests include grinding and precision machining. E-mail: caiming199004@126.com.

Bing Han, born in 1975, specializes in precision processing and special processing technology and equipment including magnetic abrasive technology and water cavitation peening technology. He obtained his Ph.D. degree in material science and engineering from *Saitama Institute of Technology*, *Japan*. He is professor at *School of Mechanical Engineering and Automation*, *University of Science and Technology Liaoning*, *China*. E-mail: hanb75@126.com.

Competing Interests
The authors declare no competing financial interests.

Author Details
[1] School of Mechanical Engineering and Automation, Northeastern University, Shenyang 110819, China. [2] School of Mechanical Engineering and Automation, University of Science and Technology Liaoning, Anshan 114051, China. [3] Beijing Linghang Kegong Education Science & Technology Company, Beijing 100084, China.

Zhao *et al. Chin. J. Mech. Eng.*   (2021) 34:3

Page 14 of 14

References

[1] J P Chen, L Gu, G J He. A review on conventional and nonconventional machining of SiC particle-reinforced aluminium matrix composites. *Advances in Manufacturing*, 2020, 8(3): 279-315.

[2] J F Wang, J L Zhao, K Y Chu. Simulation Study on Cutting Force of SiCp/A1 Composite. *Journal of System Simulation*, 2018, 30(4): 1566-1571.

[3] J F Xiang, L J Xie, F N Gao, et al. Diamond tools wear in drilling of SiCp/Al matrix composites containing Copper. *Ceramics International*, 2018, 44(5): 5341-5351.

[4] D H Xiang, Z L Shi, H R Feng, et al. Finite element analysis of ultrasonic assisted milling of SiCp/Al composites. *The International Journal of Advanced Manufacturing Technology*, 2019, 105(7-8): 3477-3488.

[5] W Zheng, Y J Wang, M Zhou, et al. Material deformation and removal mechanism of SiCp/Al composites in ultrasonic vibration assisted scratch test. *Ceramics International*, 2018, 44(13): 15133-15144.

[6] P Gu, C M Zhu, Z Tao, et al. A grinding force prediction model for SiCp/Al composite based on single-abrasive-grain grinding. *The International Journal of Advanced Manufacturing Technology*, 2020, 109(5-6): 1563-1581.

[7] F Hu, L J Xie, J F Xiang, et al. Finite element modelling study on small-hole peck drilling of SiCp/Al composites. *The International Journal of Advanced Manufacturing Technology*, 2018, 96(9-12): 3719-3728.

[8] J Xiao, S Li, S X Bai, et al. Compression brazing of SiCp/Al composite using a semisolid Zn-Al-Cu filler metal based on the strain-induced melt activation process. *JOM*, 2019, 71(12): 4931-4939.

[9] D M Wang, Z X Zheng, J Lv, et al. Multimodal particle distribution in 3D-SiC/Al-Si-Mg interpenetrating composite fabricated by pressureless infiltration. *Ceramics International*, 2018, 44(16): 19851-19858.

[10] X Wang, Y Q Li, J K Xu, et al. Comparison and research on simulation models of aluminum-based silicon carbide micro-cutting. *The International Journal of Advanced Manufacturing Technology*, 2020, 109(1-2): 589-605.

[11] H T Zha, P F Feng, J F Zhang, et al. Material removal mechanism in rotary ultrasonic machining of high-volume fraction SiCp/Al composites. *The International Journal of Advanced Manufacturing Technology*, 2018, 97(5-8): 2099-2109.

[12] S T Huang, L Guo, H H He, et al. Experimental study on SiCp/Al composites with different volume fractions in high-speed milling with PCD tools. *The International Journal of Advanced Manufacturing Technology*, 2018, 97(5-8): 2731-2739.

[13] R Sekhar, T P Singh. Mechanisms in turning of metal matrix composites: a review. *Journal of Materials Research and Technology*, 2015, 4(2): 197-207.

[14] I Ciftci, M Turker, U Seker. Evaluation of tool wear when machining SiCp-reinforced A1-2014 alloy matrix composites. *Materials and Design*, 2004, 25(3): 251-255.

[15] H A Kishawy, S Kannan. An energy based analytical force model for orthogonal cutting of metal matrix composites. *CIRP Annals - Manufacturing Technology*, 2004, 53(1): 91-94.

[16] U A Dabade, S S Joshi, R Balasubramaniam, et al. Surface finish and integrity of machined surfaces on SiCp/Al composites. *Journal of Materials Processing Technology*, 2007, 192-193(10): 166-174.

[17] Z T Bai, G B Qiu, C S Yue, et al. Crystallisation kinetics of glass-ceramics prepared from highcarbon ferrochromium slag. *Ceramics International*, 2016, 42(16): 19329-19335.

[18] Z J Wang, Q F Shu, S Sridhar, et al. Effect of P2O5 and FetO on the viscosity and slag structure in steelmaking slags. *Metall. Mater. Trans. B*, 2015, 46(2): 758-765.

[19] W Zheng, M Zhou, L Zhou, et al, Influence of process parameters on surface topography in ultrasonic vibration- assisted end grinding of SiCp/Al composites. *The International Journal of Advanced Manufacturing Technology*, 2017, 91(6): 2347-2358.

[20] J G Du, L Zhou, J G Li, et al. Analysis of chip formation mechanism in mill-grinding of SiCp/Al composites. *Materials and Manufacturing Processes*, 2014, 29(11-12): 1353-1360.

[21] S Kannan, H A Kishawy. Tribological aspects of machining aluminum metal matrix composites. *Journal of Materials Processing Technology*, 2008, 198(8): 399-406.

[22] P Feng, G Liang, J Zhang. Ultrasonic vibration-assisted scratch characteristics of silicon carbide-reinforced aluminum matrix composites. *Ceramics International*, 2014, 40(7): 10817-10823.

[23] X Zhao, Y Gong, M Cai, et al. Numerical and experimental analysis of material removal and surface defect mechanism in scratch tests of high volume fraction SiCp/Al composites. *Materials*, 2020, 12(3): 896.

[24] J Liu, K Cheng, H Ding, et al. Realization of ductile regime machining in micro-milling SiCp/Al composites and selection of cutting parameters. *Proceedings of the Institution of Mechanical Engineers Part C-Journal of Mechanical Engineering Science*, 2019, 233(12): 4336-4347.

[25] C Liu, W W Xu, J Yan, et al. Mechanistic force modeling in drilling of SiCp/Al matrix composites considering a comprehensive abrasive particle model. *The International Journal of Advanced Manufacturing Technology*, 2020, 109(1-2): 421-442.

[26] Z R Chen, C Y Li, L Xu, et al. Research on the grinding performance of high pressure sintering SiCp/Al matrix composites. *Engineering Review*, 2018, 38(2): 175-181.

[27] X L Chen, X B Wang, L J Xie, et al. Determining Al6063 constitutive model for cutting simulation by inverse identification method. *The International Journal of Advanced Manufacturing Technology*, 2018, 98(1-4): 47-54.

[28] P Wang, Z Gao, J Z Li, et al. Research on reaction brazing of Ti layer-coated SiCp/Al composites using Al-based filler metal foil. *Composite Interfaces*, 2019, 26(12): 1057-1068.

[29] T Wang, X Y Wu, G Q Zhang, et al. An experimental study on single-point diamond turning of a 55 vol% SiCp/Al composite below the ductile brittle transition depth of SiC. *The International Journal of Advanced Manufacturing Technology*, 2020, 108(7-8): 2255-2268.

[30] S T Huang, L Guo, H H He, et al. Study on characteristics of SiCp/Al composites during high-speed milling with different particle size of PCD tools. *The International Journal of Advanced Manufacturing Technology*, 2018, 95(5-8): 2269-2279.